Effect of α-nucleus potential on the ^{28}Si$(\alpha,d)^{30}$P reaction

S. K. Das,[1] A. S. B. Tariq,[1] M. A. Uddin,[1] A. S. Mondal,[1] A. K. Basak,[1] K. M. Rashid,[2] H. M. Sen Gupta,[3] and F. B. Malik[4]

[1]*Department of Physics, University of Rajshahi, Rajshahi, Bangladesh*

[2]*Department of Applied Physics and Electronics, University of Rajshahi, Rajshahi, Bangladesh*

[3]*Department of Physics, University of Dhaka, Dhaka, Bangladesh*

[4]*Department of Physics, Southern Illinois University, Carbondale, Illinois 62901*

(Received 22 December 1999; published 4 October 2000)

Microscopic and macroscopic distorted wave Born approximation calculations have been performed using molecular, Michel and normal optical potentials to analyze the angular distributions of cross sections for 12 transitions populating the 0.0, 0.709, 1.454, 1.974, 2.538, 2.72, 2.84, 3.02, 3.93. 4.62, 5.42, and 7.20 MeV states of ^{30}P via the (α,d) reaction. Only the molecular potential is able to produce satisfactory fits to the data, but the normal optical potential is found to be inadequate in accounting for the large-angle data and the Michel potential is just unsatisfactory. The spectroscopic factors for the *d*-cluster transfer are deduced from the full finite-range distorted-wave Born approximation and compared to the shell-model predictions for the even-parity states.The spin-parity assignment of the 3.93 MeV state is confirmed. The best-fit value for the finite-range parameter for the zero-range DWBA calculations is also deduced.

PACS number(s): 24.50.+g, 21.10.Jx

I. INTRODUCTION

Since the early observation of an unusual enhancement of cross section at large angles, commonly known as anomalous large angle scattering (ALAS), by Corelli *et al.* [1] in α elastic scattering by ^{16}O and ^{32}S nuclei, it has also been noted in other elastic [2–8] as well as the nonelastic [7–13] processes involving α particles. The normal optical potentials are found to be consistently inadequate in reproducing ALAS in the similar phenomena induced by α particles [13–17]. Two simple local potentials [18], with a minimum number of varying parameters, have been proposed to explain ALAS. The first one with a squared Woods-Saxon (WS) geometry, advocated by Michel and his collaborators [19–22], is a special type of optical potential, which is referred to as Michel potential [18]. The second one is a molecular type of complex potential [18,23,24] having a repulsive core in its real part. Both the potentials have been successful in reproducing ALAS in the elastic scattering of α particles [18–24] by some *sd*-shell nuclei. Nonelastic processes have so far been, in most cases, treated within the framework of direct-reaction theory using the normal optical potentials in the distorted channels, except a recent study by Das *et al.* [25] who have examined the effects of the molecular and Michel potentials in one-nucleon transfer reaction to the states of ^{28}Si.

ALAS, observed in (α,d) and (α,p) reactions on ^{28}Si [17] and (α,d) on ^{27}Al [26] have, so far, been analyzed in terms of an incoherent sum of the distorted-wave Born approximation (DWBA) contribution calculated with normal optical potentials and the compound nucleus contribution predicted on the basis of the Hauser-Feshbach model [27]. The method has, however, enjoyed a limited success. In particular, the elastic and transfer data could not be fitted with the same optical potential.

The (α,d) reaction has been shown to be a valuable spectroscopic tool for locating two-particle states [28–32]. Because of the large negative *Q*-value involved, the reaction favors the transitions to states coupled to the maximum allowed spin. Moreover, unlike the one-nucleon transfer reaction, the (α,d) reactions involving two-nucleon transfer are dependent on the coherence property, e.g., the relative signs of the different components of the wave functions. The (α,d) reactions enjoy another advantage in that these can be analyzed in terms of both the macroscopic (cluster transfer) and the microscopic approaches in the form-factor calculations. Another important feature of the (α,d) reactions lies in populating states with the $T=0$ transfer. Moreover, if the relative angular momentum of the two transferred nucleons is 0 and remains so in the reaction process only the *L*-transfer $L=J$ is allowed for the natural parity states, but two *L*-transfers $L=J\pm1$ are permitted for exciting the unnatural parity states, the spin transfer $S=1$ being unique.

The present study is undertaken to examine the influences of the normal optical, molecular and Michel potentials in analyzing the two-nucleon transfer reaction ^{28}Si$(\alpha,d)^{30}$P at 26 MeV incident energy, with the target and energy chosen for the substantial ALAS effect [18]. The latter two potentials have not been tested for a two-nucleon transfer reaction. The work is a part of a series of investigations on other nonelastic processes including the (α,t) on ^{27}Al [25], the (α,p) on ^{28}Si [33] and the (α,α') on ^{24}Mg and ^{28}Si [34] to find the nature of the α-nucleus interaction which can explain all the collision processes involving α particles. In Sec. II, the forms of the three α-nucleus potentials used in the present work are presented. The DWBA formalism and analyses are dicussed in Secs. III and IV, respectively. Section V deals with the discussion on the results of the analyses. The conclusion is given in Sec. VI.

II. α-NUCLEUS POTENTIALS

The squared WS Michel potential [20,21] including the Coulomb term $V_C(r)$ comprises of the following forms

[18,20] of the real $V_M(r)$ and imaginary $W_M(r)$ parts:

$$V_M(r) = -V_0[1+\alpha\exp\{-(r^2/\rho^2)\}] \times[1+\exp\{(r-R_R)/2a_R\}]^{-2}+V_C(r), \quad (1)$$

$$W_M(r) = -W_0[1+\exp\{(r-R_I)/2a_I\}]^{-2}, \quad (2)$$

with

$$V_C(r) = \left[\frac{Z_1Z_2e^2}{2R_C}\right]\left[3-\frac{r^2}{R_C^2}\right] \quad \text{for } r\leqslant R_C \quad (3)$$

$$= \frac{Z_1Z_2e^2}{r} \quad \text{for } r>R_C. \quad (4)$$

In Eqs. (1)–(4) $R_i = r_iA_T^{1/3}$ with $i=R$, I, and C, has been defined in terms of the usual radius parameter.

The molecular potential, which is generated from a many-body theory utilizing the energy-density functional method [23,24], has the following forms [18,24,25] for the real, $V_m(r)$, and imaginary, $W_m(r)$, parts:

$$V_m(r) = -V_0[1+\exp\{(r-R_0)/a_0\}]^{-1} + V_1\exp\{-(r^2/R_1^2)\}+V_C(r), \quad (5)$$

$$W_m(r) = -W_0\exp\{-(r^2/R_W^2)\}. \quad (6)$$

Thus, the real part is nonmonotonic with a short-range repulsion. The Coulomb and nuclear radii are scaled [18,24] according to $R_i = R_{\alpha i}+r_0A_T^{1/3}$ with $i=0,1,C,W$ and $r_0=1.35$ fm.

The normal optical potential for the alpha-nucleus system including the Coulomb term is given by [27]

$$V(r) = V_C - Vf(x_0) - i\left[Wf(x_W) - 4W_D\frac{d}{dx}f(x_D)\right], \quad (7)$$

where $f(x_i)=(1+e^{x_i})^{-1}$ with $x_i=(r-r_iA^{1/3})/a_i$ and the subscript $i=0,W$ and D.

III. THEORY OF DWBA FORMALISM

In absence of spin-orbit interactions, the differential cross-section for an (α,d) reaction on a spin-0 target with a particular J-transfer in the DWBA theory [35] is given by

$$\frac{d\sigma}{d\Omega} = \frac{\mu_i\mu_f}{(2\pi\hbar^2)^2}\frac{k_f}{k_i}(2J+1) \times\sum_{LM}\left|\sum_{\rho_1\rho_2}\beta^{1/2}[\rho_1\rho_2;J0]\begin{bmatrix} l_1 & l_2 & L\\ \frac{1}{2} & \frac{1}{2} & 1\\ j_1 & j_2 & J\end{bmatrix}B_M^L\right|^2, \quad (8)$$

where μ's and k's are, respectively, the reduced masses and wave numbers. The subscripts i and f refer to the incident and outgoing channels, respectively. $\rho_1=[n_1l_1j_1]$ and $\rho_2=[n_2l_2j_2]$ denote the orbital quantum numbers for the transferred nucleons in the final nucleus. $\beta^{1/2}[\rho_1\rho_2;J0]$ are the spectroscopic amplitudes in the jj-coupling for an angular momentum transfer J and an isospin transfer $T=0$. The large square bracket in Eq. (8) refers to the normalized 9-j symbol, with LS-jj transformation factor [36]. B_M^L describes the kinematical aspects of the reaction. In Eq. (8) the light particle spectroscopic factor $c^2s=1.0$ for (α,d) reactions has been used.

In the macroscopic DWBA calculations, no information on the structure of the cluster is required except the quantum numbers (N,L) is defined by

$$2(n_1+n_2)+l_1+l_2=2N+L, \quad (9)$$

where the quantum numbers $\nu=0$ and $\lambda=0$ are assumed for the relative $0s$-state internal motion of the transferred cluster. The expression for cross section in terms of the cluster quantum numbers (N,L) is given by [36]

$$\frac{d\sigma}{d\Omega} = \frac{\mu_i\mu_f}{(2\pi\hbar^2)^2}\frac{k_f}{k_i}(2J+1)\sum_{LM}|G_{LJ}\mathrm{Re}\,{}_M^L|^2. \quad (10)$$

In Eq. (10), only one N value is considered to contribute, the two nucleons in the cluster being in the relative $0s$ state. The structure amplitude G_{LJ}, as defined by Glendenning [36] is expressed as

$$G_{LJ} = \sum_{\rho_1\rho_2}(2-\delta_{\rho_1\rho_2})^{1/2}\beta^{1/2}[\rho_1\rho_2;J0]\begin{bmatrix} l_1 & l_2 & L\\ \frac{1}{2} & \frac{1}{2} & 1\\ j_1 & j_2 & J\end{bmatrix} \times\Omega_{00}\langle 00,NL:L|n_1l_1,n_2l_2:L\rangle. \quad (11)$$

In Eq. (11), Ω_{00} denotes the overlap of the spatial wave function of relative motion of the two particles in the transferred cluster with the corresponding part in the incident α particle. $\langle|\rangle$ represents the Brody-Moshinsky bracket [35–37].

Denoting the macroscopic cross sections calculated for the L-transfer with the FFR code DWUCK5 [38] by $(d\sigma/d\Omega)_{\mathrm{DW5}}^L$ and taking advantage of the incoherent sum over the L-transfer(s) as in Eqs. (8) and (10), one can write the experimental cross sections for this reaction as

$$\left(\frac{d\sigma}{d\Omega}\right)_{\mathrm{expt}} = (2J+1)\left[A_{L1}\left(\frac{d\sigma}{d\Omega}\right)_{\mathrm{DW5}}^{L1}+A_{L2}\left(\frac{d\sigma}{d\Omega}\right)_{\mathrm{DW5}}^{L2}\right]. \quad (12)$$

On the other hand, the experimental cross sections are related to the microscopic cross sections $(d\sigma/d\Omega)_{\mathrm{DW4}}^L$ calculated with the ZR code DWUCK4 [38] by

$$\left(\frac{d\sigma}{d\Omega}\right)_{\mathrm{expt}} = \aleph\left(\frac{d\sigma}{d\Omega}\right)_{\mathrm{DW4}}. \quad (13)$$

TABLE I. Potential parameters for DWBA calculations. The potential depth V for the bound states is adjusted to give the separation energy.

Channel		$\alpha + {}^{28}$Si		$d + {}^{30}$P	$d+d$	$d + {}^{28}$Si
Potential type	Molecular [a]	Michel [a]	Optical [b]	Optical [c]	Bound state [a]	
V_0 (MeV)	26.0	21.0	50.42	102.7	V	V
R_0 (fm)	5.35	5.00				
r_0 (fm)			1.699	1.07	1.05	0.935
a_0 (fm)	0.34	0.60	0.505	0.852	0.50	0.997
V_1 (MeV)	42.0					
R_1 (fm)	2.80					
α		5.82				
ρ (fm)		6.25				
W_0 (MeV)	15.0	28.9	10.34			
R_W (fm)	4.0	3.85				
r_I (fm)			1.699			
a_I (fm)		0.65	0.505			
W_D (MeV)				16.10		
r_D (fm)				1.53		
a_D (fm)				0.574		
V_{SO} (MeV)				6.0		
r_{SO} (fm)				1.07		
a_{SO} (fm)				0.852		
r_C (fm)		1.30	1.30	1.15	1.25	1.3
R_C (fm)	9.35					

[a]Reference [18].
[b]Reference [17].
[c]Reference [40].

$\aleph$ in Eq. (13) is the normalization constant for the (α,d) reactions. The form of Eq. (12) shows that A_{L1} and A_{L2} are the spectroscopic factors [26,32] for the $L1$ and $L2$ transfers, respectively. The spectroscopic factor [26] A_L in Eq. (12) for each of the L transfers and the normalization constant $\aleph$ in Eq. (13) can be extracted from fitting the experimental cross sections.

IV. DWBA ANALYSIS

The microscopic zero-range and macroscopic full finite-range (FFR) DWBA calculations for the angular distributions have been performed using the computer codes DWUCK4 and DWUCK5 [38], respectively. Both the codes are modified to include the Michel potential. Corrections due to nonlocality [38,39] of potentials in the conventional form have been applied using the nonlocality parameters $\beta(\alpha) = 0.2$ and $\beta(p) = 0.85$ fm. In both the microscopic ZR and macroscopic FFR calculations, the molecular, Michel, and normal optical types of α-^{28}Si potential and the optical d-^{30}P potential have been employed. The parameters of the molecular and Michel potentials are taken from the work of Tariq *et al.* [18], and those of the normal optical potentials for the incident channel are from Jankowski *et al.* [17]. Several sets of the d-^{30}P optical potentials including that from Ref. [17] have been tried, but the one from the work of Fitz *et al.* [40] produces the best fit. All the potential parameters employed in the present analyses are displayed in Table I.

A. Macroscopic DWBA calculations

The macroscopic analyses have been performed using the full finite-range DWBA code DWUCK5 [38]. The bound-state geometries for the d-d and d-^{28}Si Woods-Saxon (WS) potentials, shown in Table I, are taken from [17]. The bound state wave functions for the transferred deuteron in alpha as well as the final nucleus have been generated by adjusting the deuteron separation energies. At the start of calculations, the accuracy parameters used in the code DWUCK5 have been assigned appropriate values, to define effective width of wave numbers [38,41] in the expansion of the distorted waves in terms of plane waves for making the zero-range calculations identical to those from the code DWUCK4 [38]. This ensures the necessary *covergence* for the integral for the zero-range form factor, defined in Eq. (3.9) of Charlton [41].

The cluster configurations of the transferred deuteron for the different states of excitation are shown in Table II. For the final states with natural parity, populated by one L transfer, the DWBA predictions are normalized to the data to yield the relevant spectroscopic factor A_L as defined in Eq. (12). On the other hand, for the transitions involving two L transfers, leading to the final states with unnatural parity, the spectroscopic factors are obtained by minimizing the value of χ^2 defined by

$$\chi^2 = \sum_i \left[\frac{\sigma_{\rm expt}(\theta_i) - \sigma_{\rm DW}(\theta_i)}{\Delta\sigma_{\rm expt}(\theta_i)} \right]^2, \qquad (14)$$

TABLE II. Cluster specstroscopic factors are compaared to the theoretical shell-model factors for the FPSDI, CW, and MSDI interactions. FPSDI and CW spectroscopic factors are taken from Ref. [32]. MSDI factors are calculated from the spectroscopic amplitudes $\beta^{1/2}$ of Ref. [17] by the method outlined in Ref. [32]. S_L values are normalized to the value of $|G_{67}^{7.20}|^2$ for the 7.20 MeV state.

E_x	J^π	Cluster configuration	Cluster spectroscopic factor			Shell model spectroscopic factor $S_L=\|G_{LJ}\|^2/\|G_{67}^{7.20}\|^2$		
(MeV)		N,L	A_L [a]	A_L [b]	A_L [c]	FPSDI	CW	MSDI
0.0	1^+	2,0	0.23±0.07	1.76±0.20	0.28	0.448	0.043	0.168
		1,2	0.23±0.07	[d]	0.56	0.237	0.121	0.031
0.709	1^+	2,0	0.16±0.07	1.45±0.20		0.029	0.030	0.020
		1,2	0.24±0.08	[d]	0.85	0.617	0.274	0.038
1.454	2^+	1,2	0.25±0.05	0.20±0.04	0.32	0.372 [a]	0.081	7.8×10^{-4}
1.974	3^+	1,2	0.11±0.04	0.72±0.13		0.041	0.078	0.004
		0,4	0.09±0.03	0.47±0.20		6.1×10^{-4}	0.134	1.5×10^{-3}
2.538	3^+	1,2	0.16±0.04	0.67±0.14		0.015	0.165	
		0,4	0.07±0.03	<0.25		0.426	0.076	
2.72	2^+	1,2	0.28±0.05	0.12±0.02	0.34	0.058	0.045	
2.84	3^+	1,2	0.08±0.02	0.16±0.07		0.007	0.007	
		0,4	0.09±0.02	0.33±0.11		0334	0.254	
3.02	1^+	2,0	0.03±0.02	0.51±0.15	0.27	9.7×10^{-4}	0.319	
		1,2	0.32±0.05	0.06±0.10	0.35	1.4×10^{-3}	0.021	
3.93	2^-	2,1	0.11±0.04		0.32			
		1,3	0.18±0.04					
	(3^+)	(1,2)	(0.06±0.05)	(0.14±0.05)				
		(0,4)	(0.08±0.05)	(0.05±0.06)				
4.62	3^-	2,1	0.15±0.04	0.17±0.02	0.30			
5.42	2^-	2,1	0.54±0.09					
		1,3	0.06±0.03		0.86			

[a]Present work.
[b]Reference [32].
[c]Reference [17].
[d]Too small a value to quote.

where $\sigma_{\rm expt}(\theta_i)=(d\sigma/d\Omega)_{\rm expt}(\theta_i)$ and $\Delta\sigma_{\rm expt}(\theta_i)$ are, respectively, the experimental cross section, as defined in Eq. (12), and its error at the scattering angle θ_i. $\sigma_{\rm DW}(\theta_i)$ is the cross section predicted by the DWBA theory.

The DWBA predictions with the molecular (solid curves), normal optical (broken curves), and Michel (dotted curves) potentials are compared to the data of the ground (1^+), 0.709 (1^+), 1.454 (2^+), 2.72 (2^+), and 3.02 MeV (2^+) states in Fig. 1; to the data of the 1.974 (3^+), 2.538 (3^+), and 2.84 MeV (3^+) in Fig. 2; and to the data of the 3.93 (2^-), 4.63 (3^+), and 5.42 MeV (2^+) states of ^{30}P in Fig. 3. It is amply clear from Figs. 1–3 that the calculations with the molecular potential produces the best fits to data for all the transitions. Furthermore, the Michel potential generates cross sections, which are lower by 1 to 2 orders of magnitude than those predicted by either the normal optical or the molecular potential. Table III gives the comparison of the total spectroscopic factors for the cluster transfer for the three types of potentials.

The compiled work of Endt and van der Leun [44] suggests alternative spin parity for the 3.93 MeV state as $J^\pi=1^+$, 2^-, or 3^+. While de Meijer *et al.* [32] assigned $J^\pi=3^+$ for the state, Jankowski *et al.* [17] suggested 2^-. The DWBA calculations with the molecular potential for both

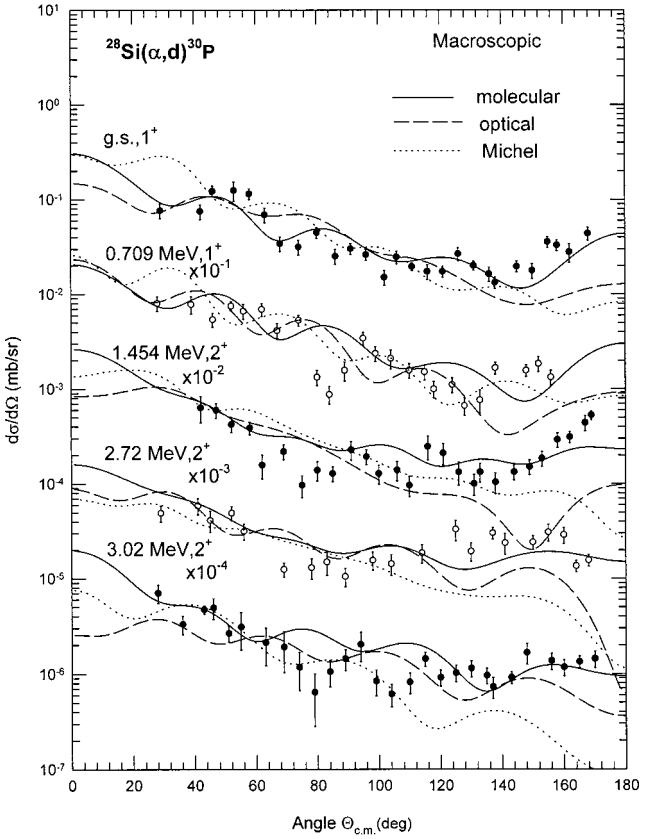

FIG. 1. Comparison of the full finite-range macroscopic DWBA calculations for the ^{28}Si$(\alpha,d)^{30}$P reaction at 26 MeV leading to the 1^+ and 2^+ states of ^{30}P to the differential cross section data. The solid, broken, and dotted curves are the predictions using the molecular, normal optical, Michel α-^{28}Si potential, respectively. The data are from [17].

$J^\pi = 2^-$ and 3^+ are compared to the experimental cross sections in Fig. 4. The $J^\pi = 2^-$ assignment is clearly favored, confirming the observation of Jankowski *et al.*

B. Microscopic DWBA calculations

The microscopic calculations have been performed using the zero-range code DWUCK4 for the positive parity states with the transferred particles stripped to the sd-shell. The present analyses make use of three sets of spectroscopic amplitudes $\beta^{1/2}$, two sets based on the FPSDI and MSDI Hamiltonians as defined in Wildenthal *et al.* [42] and the shell-model wave functions of the ^{28}Si and ^{30}P nuclei given by Wildenthal *et al.* [42,43] and the third one, labeled by CW [32], derived from the wave functions of Chung and Wildenthal referred to in [32]. The FPSDI and CW amplitudes are taken from de Meijer *et al.* [32], while the MSDI amplitudes are from Jankowski *et al.* [17]. All the three sets of spectroscopic amplitudes are calculated in the model space of $0d_{5/2}$-$1s_{1/2}$-$0d_{3/2}$. Since the codes DWUCK4 and DWUCK5 assume that the spherical harmonics carry a time reversal phase of i^l, a factor not used in the phase conventions adopted in the calculations of the spectroscopic amplitudes

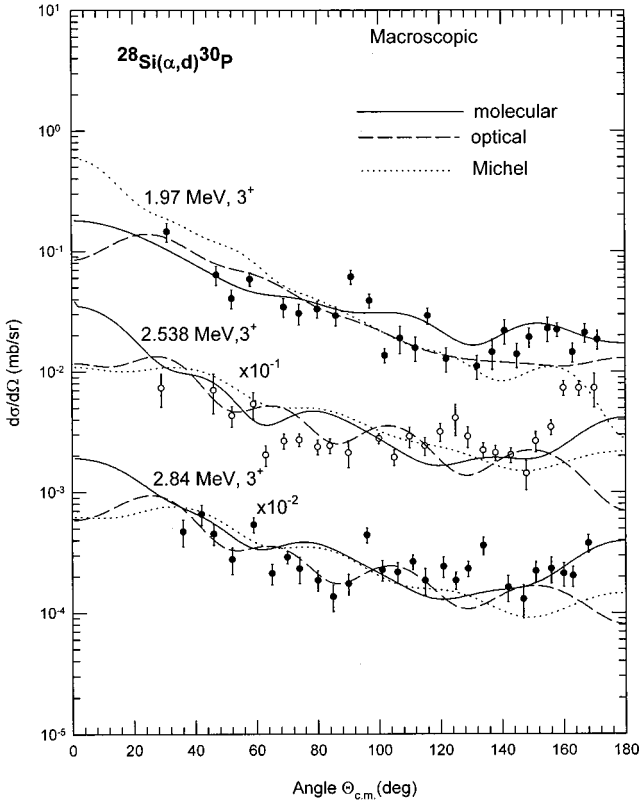

FIG. 2. Same as in Fig. 1 for the transition to the 3^+ states of ^{30}P.

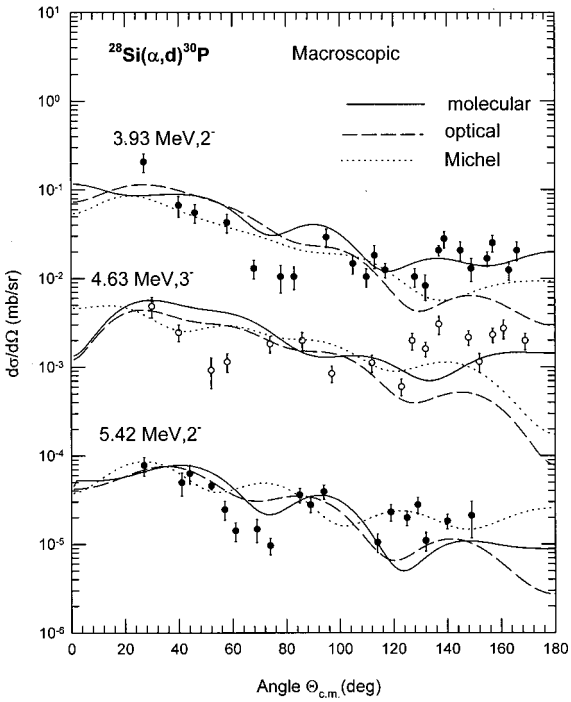

FIG. 3. Same as in Fig. 1 for the transition to the 2^- and 3^- states of ^{30}P.

TABLE III. Comparison of deduced total specstroscopic factors from the macroscopic and normalization factors for the microscopic FPSDI calculations using the molecular, normal optical, and Michel potentials. Total spectroscopic factor is the sum of the spectroscopic factors for the two L transfers for the unnatural parity states.

			Total spectroscopic factors			Normalization constant ℵ		
			Macroscopic calculations			Microscopic calculations		
E_x (MeV)	J^π	L	Molecular	Optical	Michel	Molecular	Optical	Michel
0.0	1^+	0+2	0.46	0.74	23.4	280	480	7000
0.709	1^+	0+2	0.40	1.33	30.0	70	85	8000
1.454	2^+	2	0.25	0.50	11.0	270	950	1800
1.974	3^+	2+4	0.20	0.57	20.0	1500	2000	35000

[32], the amplitudes have been multiplied by an extra phase of $i^{l_1+l_2-L}$ before feeding these to the codes.

The bound state wave functions for each of the transferred nucleons have been generated by assuming a real Woods-Saxon well with the geometry parameters $r_0=1.25$ fm and $a_0=0.65$ fm and the depth adjusted to produce the binding energy equal to half the separation energy of the transferred deuteron. A Thomas-Fermi spin-orbit term with $\lambda=25$ has also been used for the bound state wave functions.

A Gaussian form of finite range correction in the local energy approximation [38] has been investigated. Figure 5 compares the microscopic DWBA calculations for the molecular type of α-^{28}Si potential using the range parameter $R=0.0$ fm (broken curves), 0.7 fm (solid curves) and 0.85 fm (dotted curves) to the experimental data for the transfer to the ground (1^+), 2.53 (3^+), 2.84 (3^+), and 3.02 MeV (2^+) states. The finite-range correction with $R=0.7$ fm improves the fits to the data.

The effect of the three types of the α-^{28}Si potential on the microscopic DWBA calculations has also been examined using the spectroscopic amplitudes calculated from the FPSDI interaction. Figure 6 displays the DWBA predictions for the molecular (solid curves), normal optical (broken curves) and Michel (dotted curves) potentials, which are compared to the data for the ground (1^+), 0.71 (1^+), 1.45 (2^+), and 1.97 MeV (3^+) states of ^{30}P. As in the case of the macroscopic analyses, the molecular potential provides the best description of the data and the Michel gives the worst. Moreover, the predicted cross sections with the Michel potential are so small that they need normalization factors (Table III), larger by orders of magnitude, compared to those for the molecular and normal optical potentials.

Figures 7 and 8 display the comparison of the microscopic DWBA calculations with the finite-range parameter

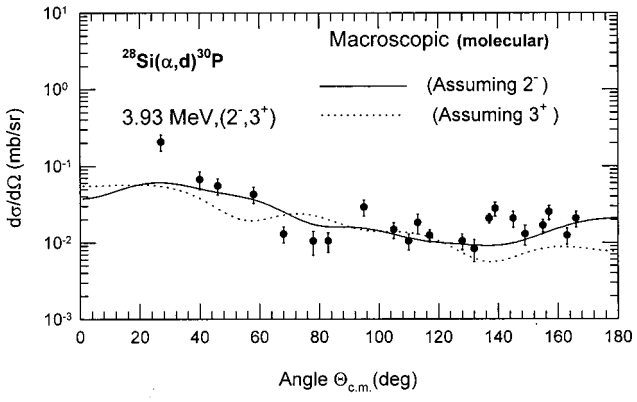

FIG. 4. Full finite-range macroscopic DWBA calculations using the molecular α-^{28}Si potential for the 3.93 MeV state assuming the spin-parity $J^\pi=2^-$ (solid curve) and 3^+ (dotted curve) are compared to the data. The data are from [17].

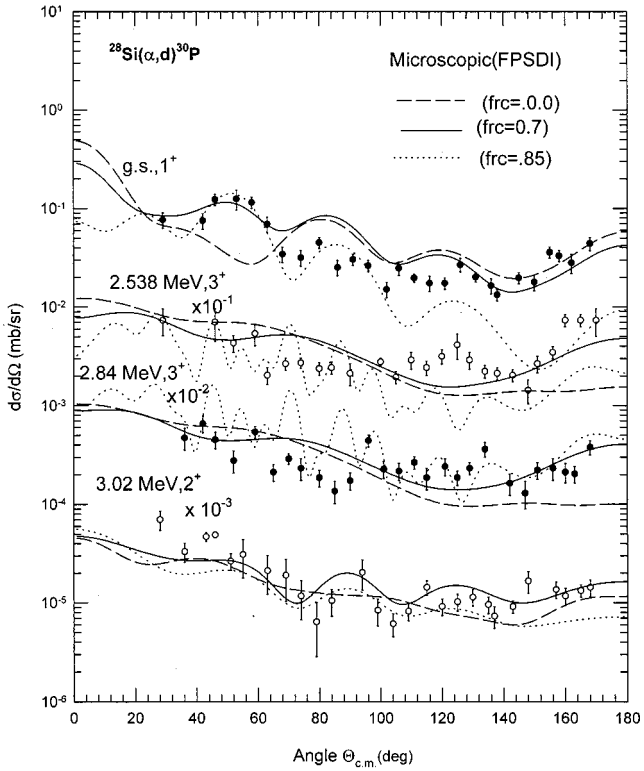

FIG. 5. Comparison of the zero-range microscopic DWBA calculations using the FPSDI spectroscopic amplitudes and the molecualr potential in the α channel for the ^{28}Si$(\alpha,d)^{30}$P reaction at 26 MeV leading to the ground (1^+), 2.538 (3^+), 2.84 (3^+), and 3.02 MeV (2^+) states of ^{30}P to the differential cross section data. The solid curves are the predictions using the finite-range (FR) correction with FR parameter $R=0.7$ fm. The broken and dotted curves are the predictions with $R=0.0$ and 0.85 fm, respectively. The data are from [17].

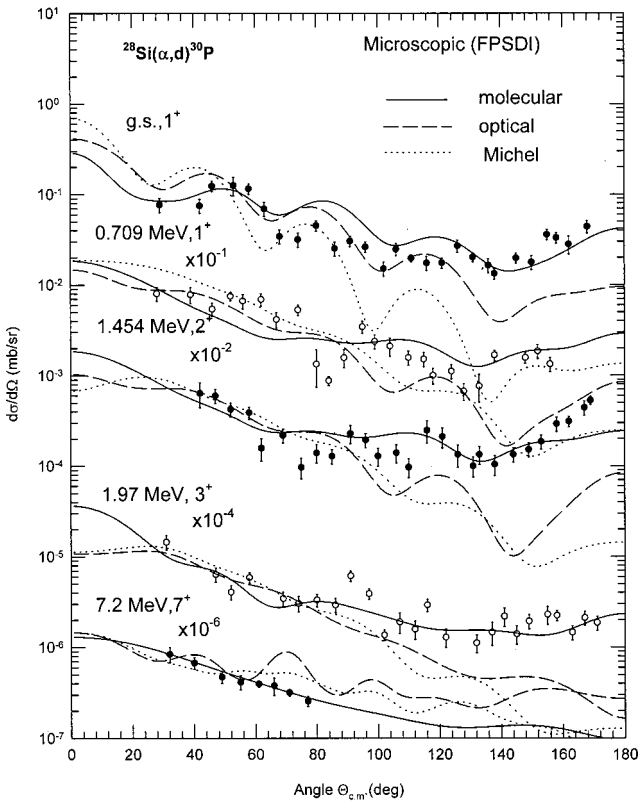

FIG. 6. Comparison of zero-range microscopic DWBA calculations with FR correction for the ^{28}Si$(\alpha,d)^{30}$P reaction at 26 MeV leading to the ground (1^+), 0.709 (1^+), 1.454 (2^+), 1.97 (3^+), and 7.20 MeV (7^+) states of ^{30}P to the differential cross section data. The solid, broken, and dotted curves are the predictions using the molecular, normal optical, and Michel α-^{28}Si potential, respectively. The data are from [17].

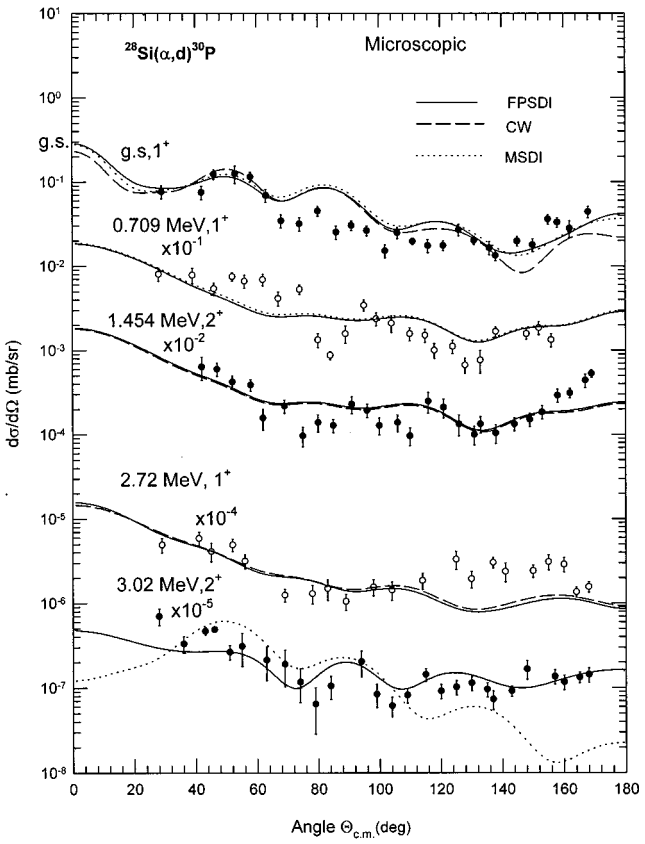

FIG. 7. Comparison of zero-range microscopic DWBA calculations with Fr correction and the molecular potential for the ^{28}Si$(\alpha,d)^{30}$P reaction at 26 MeV leading to the 1^+ and 2^+ states of ^{30}P to the differential cross section data. The solid, broken, and dotted curves are the predictions using the FPSDI, CW, and MSDI spectroscopic amplitudes. The data are from [17].

$R=0.7$ fm and the molecular α-^{28}Si potential, for the FPSDI (solid curves), CW (broken curves), and MSDI (dotted curves) interactions. The calculations with the three interactions produce more or less the same quality of fits to the transfer data to the ground (1^+), 0.709 (1^+), 1.454 MeV (2^+) states (Fig. 7). The FPSDI and CW amplitudes produce identical predictions for the 2.72 MeV (2^+) state (Fig. 7) and 2.84 MeV (3^+) state (Fig. 8) and the same quality of fits to the 1.97 (3^+) and 2.538 (3^+) MeV states (Fig. 8). For the 3.02 MeV state, FPSDI gives a better description at large scattering angles than CW does (Fig. 7). Nonetheless, the spectroscopic amplitudes from the three interactions produce completely different spectroscopic factors S_L, as listed in Table II. Moreover, the experimental cross sections for the reaction leading to the ground (1^+), 0.709 (1^+), 1.454 (2^+), 1.974 (3^+), 2.538 (3^+), 2.72 (2^+), 2.84 (3^+), and 3.02 MeV (1^+) states of ^{30}P, need normalization constants as listed in Table IV, which are widely different and inconsistent.

The 7.20 MeV (7^+) state is considered to have a pure stretched $(0f_{7/2})^2$ configuration leading to the spectroscopic amplitude for the (α,d) reaction as $\beta^{1/2}=1.0$ [30,32]. This model independent value of $\beta^{1/2}$ has been used to deduce the normalization constant for the reaction as $\aleph=722\pm25$, which compares closely with $\aleph=870\pm20$ and 650 ± 20 obtained, following two methods for calculating the form factors, by de Meijer *et al.* [32]. But only a few of the extracted $\aleph$ values for other states given in Table IV are close to the model independent value, deduced from the reaction data for the 7.20 MeV state. None of the FPSDI, CW, and MSDI interactions produce a consistent set of values for the normalization constant.

C. Spectroscopic factors

The model dependent spectroscopic factors are calculated from the FPSDI, CW, and MSDI spectroscopic amplitudes $\beta^{1/2}$ by the method outlined in [32]. Since the spectroscopic factor for the 7.20 MeV state is unity, the spectroscopic factors for other transitions are obtained by

$$S_L=\frac{|G_{LJ}|^2}{|G_{67}(7.20)|^2}, \tag{15}$$

where the structure factor G_{LJ} is expressed through Eq. (11) and $G_{67}(7.20)=0.56\Omega_{00}$ denotes the value of the structure factor for the 7.20 MeV state. The S_L values, which are listed in Table II, are taken from de Meijer *et al.* [32] for the

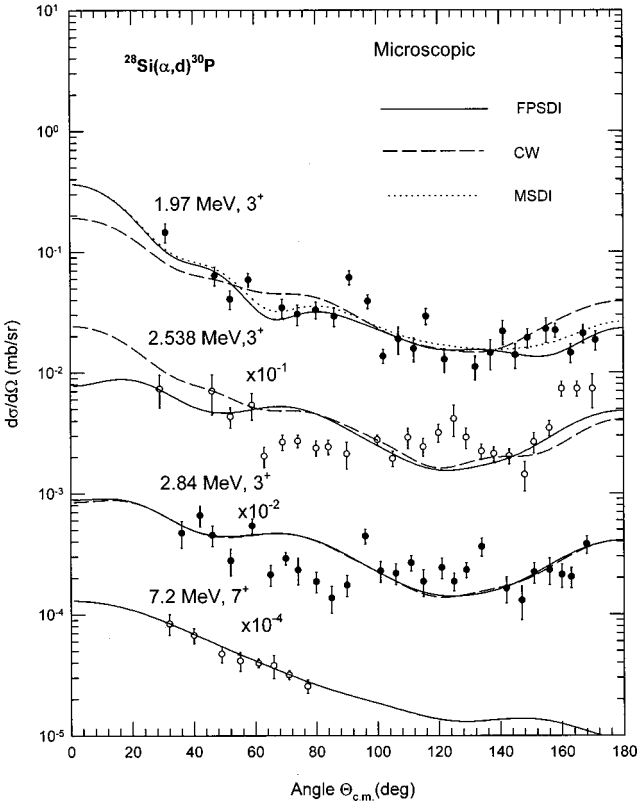

FIG. 8. Same as in Fig. 7 for transition to the 3^+ and 7^+ states of ^{30}P.

FPSDI and CW spectroscopic amplitudes. For the MSDI interaction, the S_L values are calculated using Eq. (15) from the MSDI spectroscopic amplitudes from Jankowski *et al.* [17]. The theoretical spectroscopic factors S_L are compared to the experimental spectroscopic factors A_L, deduced from the macroscopic analysis in Table II.

V. DISCUSSION

In the present work, both the molecular and Michel types of α-nucleus potential have been used, for the first time, for the analyses of two-nucleon transfer data. The data for the even-parity states up to $E_x = 3.02$ MeV, have been analyzed both in terms of the FFR DWBA with the cluster form factor and the ZR DWBA with the microscopic form factors. In the latter calculations, the FPSDI and CW [32] as well as MSDI [17] spectroscopic amplitudes derived from the wave functions of Wildenthal and his collaborators [42,43] and Ref. [20] cited in the work of de Meijer *et al.* [32]. The data of the odd-parity states are analyzed only in terms of the macroscopic FFR calculations.

In both microscopic and macroscopic DWBA calculations, the molecular potential (Figs. 1–3 and 7,8) produces the best description of the data for all the transitions studied. The Michel potential, which has been shown to describe satisfactorily the elastic $\alpha + ^{28}$Si data [18], is found inadequate not only in accounting for the pattern of the angular distributions (Figs. 1–3, 6), but also in reproducing the right order of magnitude for the cross section data. The normal optical potential, on the other hand, which can fit the angular distribution at forward scattering angles and predicts the same order of cross sections as the molecular one does, is found inadequate in describing the data at large scattering angles (Figs. 1–3, 6).

The finite-range correction to the ZR microscopic calculations produces substantial effects on the pattern of the angular distributions and improves substantially the fits to the data as can be seen in Fig. 5. This confirms the observation made by Bencze and Zimanyi [45]. The best fit value for the finite-range parameter found is $R = 0.70$ fm for the reaction.

In the literature, an ambiguity in the spin-parity assignment for the 3.93 MeV state is noted. The comparison of the macroscopic DWBA predictions for $J^\pi = 2^-$ (solid curve) and 3^+ (dotted curve) in Fig. 4 to the experimental data favors the former, confirming the assignment of Jankowski *et al.* [17] and contradicting that of de Meijer *et al.* [32].

The spectroscopic factors A_L for the transitions to the final states up to $E_x = 5.42$ MeV are deduced by comparing the macroscopic DWBA calculations to the data. Table II compares the deduced spectroscopic factors A_L to those obtained at 50 MeV incident energy by de Meijer *et al.* [32] and those extracted using the same data as of the present work by Jankowski *et al.* [17]. The results of Jankowski *et al.* are not reliable as they included the compound nucleus contributions in their analyses. The results of de Meijer *et al.*

TABLE IV. Normalization constant $\aleph$ for the microscopic zero-range calculations for different shell-model interactions. $\aleph_{rel}$ is the value relative to the model independent $\aleph = 722$ for the 7.20 MeV state.

E_x (MeV)	J^π	L	Normalization constant $\aleph$ Interaction			Relative normalization constant $\aleph_{rel}$ Interaction		
			FPSDI	CW	MSDI	FPSDI	CW	MSDI
0.0	1^+	0+2	280	4000	800	0.388	5.540	1.108
0.709	1^+	0+2	70	180	1500	0.096	0.249	2.08
1.454	2^+	2	270	850	5500	0.374	1.177	7.618
1.974	3^+	2+4	1500	500	7000	2.077	0.692	9.965
2.538	3^+	2+4	220	900		0.304	1.246	
2.72	2^+	2	550	4500		0.762	6.233	
2.84	3^+	2+4	350	450		0.484	0.623	
3.02	1^+	0+2	14000	450		19.39	0.623	

are based on the zero-range calculations. Nevertheless, their A_L values for the transitions involving one L-transfer leading to, particularly, the 1.454 (2^+) and 4.62 MeV (3^-) states are remarkably close to those of the present work.

The A_L values for the even-parity states and the model dependent theoretical spectroscopic factors S_L, defined in Eq. (15), are compared in Table II. It can be noticed that apart from the ground state (1^+), 1.454 (2^+), and 2.72 MeV (2^+) transitions, the total spectroscopic factors ΣA_L agree with ΣS_L for the CW interactions. On the other hand, the FPSDI predictions for ΣS_L values are closer to the experimental ΣA_L for the ground and 1.45 MeV states. Neither of the FPSDI and CW interactions reproduces the experimental A_L for the 2.72 MeV state. It can also be noticed from Table III that FPSDI yields larger spectroscopic strengths compared to CW. This is also reflected in the deduced values of relative normalization constants $\aleph_{\rm rel}$ in Table IV, where FPSDI needs in general smaller $\aleph$ values to get to the data. None of the three interactions, viz. FPSDI, CW, and MSDI, is able to yield consistent values to account for the even-parity states. However, the model-independent $\aleph = 722 \pm 25$ is obtained from the data of the 7.20 MeV (7^+) state, where the spectroscopic amplitude is believed to be unity.

VI. CONCLUSION

Both the macroscopic and microscopic DWBA analyses suggest that the molecular type of the α-^{28}Si potential is undoubtedly the best of the three types of potentials considered. The success of the present analyses lies in observing that the experimental cross sections for all the transitions are reproduced over the entire angular range without the addition of compound nucleus contributions, which are unlikely to happen at the incident energy considered herein.

The present work in conjunction with the previous studies of the α-elastic scattering on ^{24}Mg and ^{28,30}Si by Tariq *et al.* [18], of the (α,t) reaction on ^{27}Al [25] and the (α,p) reaction on ^{28}Si [33] by Das *et al.*, and of the α-inelastic scattering on ^{24}Mg and ^{28}Si by Rahman *et al.* [34] confirms that the molecular potential is the best of the three types of α-nucleus interactions including the Michel and the normal optical potentials, in describing the elastic, inelastic and rearrangement collision processes on the sd-shell nuclei. This ushers in hopes for finding a global α-nucleus potential, as observed by Hodgson [46]. It remains to be examined whether the molecular type of potentials are capable of accounting for collision processes involving α particle and other light and medium-light nuclei. For this purpose, it would be extremely helpful to have complete angular distributions for different processes involving a particular nucleus.

ACKNOWLEDGMENTS

This work was partly supported by Grant No. INT-9808892 of the U.S. National Science Foundation and a grant from the Ministry of Science and Technology, Government of Bangladesh, which are thankfully acknowledged. One of the authors, S.K.D., is thankful to Shahjalal University of Science and Technology, Bangladesh for the study leave grant. The authors are also thankful to Professor P.D. Kunz of the University of Colorado for making the codes DWUCK4 and DWUCK5 available to them.

[1] J.C. Correlli, E. Bleuler, and D.J. Tendam, Phys. Rev. **116**, 1184 (1959).
[2] C.R. Gruhn and N.S. Wall, Nucl. Phys. **81**, 161 (1966).
[3] G. Gaul, H. Lüdeke, R. Santo, H. Schmeing, and R. Stock, Nucl. Phys. **A137**, 177 (1969).
[4] A. Bobrowska, A. Budzanowski, K. Grotowski, L. Jarczyk, S. Micek, H. Niewodniczanski, A. Strzalkowski, and Z. Wróbel, Nucl. Phys. **A126**, 361 (1969).
[5] H. Eickhoff, D. Frekers, H. Lönner, K. Poppensieker, R. Santo, G. Gaul, C. Mayer-Böricke, and P. Turek, Nucl. Phys. **A252**, 333 (1975).
[6] H. Abele, H.J. Hauser, A. Körber, W. Leitner, R. Neu, H. Plappert, T. Rohwer, G. Staudt, M. Straßer, S. Welte, M. Walz, P.D. Eversheim, and F. Hinterberger, Z. Phys. A **326**, 373 (1987).
[7] W. Trombik, K.A. Eberhard, and J.S. Eck, Phys. Rev. C **11**, 685 (1975).
[8] A.M. Kobos, B. A. Brown, R. Lindsay, and G.R. Satchler, Nucl. Phys. **A425**, 205 (1984).
[9] H. Oeschler, H. Schroter, H. Ficjs, L. Baum, G. Gaul, H. Ludechi, R. Santo, and R. Stock, Phys. Rev. Lett. **28**, 694 (1972).
[10] Å. Bredbacka, M. Brenner, K.-M. Källman, P. Månngard, Z. Máté, S. Szilágyi, and L. Zolnai, Nucl. Phys. **A574**, 397 (1994).
[11] L. Jarczyk, B. Maciuk, M. Siemaszko, and W. Zipper, Acta Phys. Pol. B **7**, 531 (1976).
[12] H.-J. Apell, W. Gemeinhardt, R. Stock, R.R. Betts, O. Hansen, A. Sperduto, H. Fuchs, and R. Santo, Nucl. Phys. **A246**, 477 (1975).
[13] A.W. Obst and K.W. Kemper, Phys. Rev. C **6**, 1705 (1972).
[14] H. Kitazawa, Y. Harima, and N. Mukai, Nucl. Phys. **A510**, 429 (1990).
[15] B. Xiumin, L. Shiming, W. Yuanda, Y. Rongfang, H. Bingyin, and S. Zuxun, Chin. Phys. **6**, 645 (1986).
[16] A.E. Antropov, S.I. Vasilev, P. Zurabin, and B.N. Orlov, Izv. Akad. Nauk SSSR, Ser. Fiz. **38**, 2175 (1974); **37**, 1873 (1973).
[17] K. Jankowski, A. Grzeszczuk, M. Siemaszko, A. Surowiec, W. Zipper, A. Budzanowski, and E. Kozik, Nucl. Phys. **A426**, 1 (1984).
[18] A.S.B. Tariq, A.F.M.M. Rahman, S.K. Das, A.S. Mondal, M.A. Uddin, A.K. Basak, H.M. Sen Gupta, and F.B. Malik, Phys. Rev. C **59**, 2558 (1999).
[19] Th. Delbar, Gh. Grégoire, G. Paic, R. Ceuleneer, F. Michel, R. Vanderpoorten, R. Budzanowski, H. Dabrowski, L. Friendl, K. Grotoski, S. Micek, R. Planeta, A. Strzalkowski, and A. Eberhard, Phys. Rev. C **18**, 1237 (1978).
[20] F. Michel, J. Albinski, P. Belery, Th. Delbar, Gh. Grégoire, B. Tasiaux, and G. Reidemeister, Phys. Rev. C **28**, 1904 (1983).

[21] F. Michel, G. Reidemeister, and S. Ohkubo, Phys. Rev. Lett. **57**, 1215 (1986).
[22] F. Michel, G. Reidemeister, and Y. Kondo, Phys. Rev. C **51**, 3290 (1995).
[23] I. Reichstein and F.B. Malik, Phys. Lett. **37B**, 344 (1971).
[24] P. Manngård, M. Brenner, M.M. Alam, I. Reichstein, and F.B. Malik, Nucl. Phys. **A504**, 130 (1989).
[25] S.K. Das, A.S.B. Tariq, A.F.M.M. Rahman, P.K. Roy, M.N. Huda, A.S. Mondal, A.K. Basak, H.M. Sen Gupta, and F. B. Malik, Phys. Rev. C **60**, 044617 (1999).
[26] I. Skwirczynska, E. Kozik, A. Budzanowski, J. Ploskonka, and A. Strzalkowski, Nucl. Phys. **A371**, 288 (1981).
[27] W. Hauser and H. Feshbach, Phys. Rev. **87**, 366 (1952).
[28] H. Nann, W.S. Chien, A. Saha, and B.H. Wildenthal, Phys. Lett. **60B**, 32 (1975).
[29] A. Van der Woude and R.J. de Meijer, Nucl. Phys. **A258**, 199 (1976).
[30] R.M. Del Vecchio, R.T. Kouzes, and R. Sherr, Nucl. Phys. **A265**, 220 (1976).
[31] H. Nann, W.S. Chien, A. Saha, and B.H. Wildenthal, Phys. Rev. C **15**, 1959 (1977).
[32] R.J. de Meijer, L.W. Put, J.J. Akerman, J.C. Vermeulen, and C.R. Binham, Nucl. Phys. **A386**, 200 (1982).
[33] S.K. Das, A.K. Basak, K. Banu, A.S. Mondal, A.S.B. Tariq, A.F.M.M. Rahman, H.M. Sen Gupta, and F.B. Malik, Phys. Rev. C **62**, 054606 (2000), following paper.
[34] A.F.M.M. Rahman, A.S. Mondal, S.K. Das, A.S.B. Tariq, A.K. Basak, H.M. Sen Gupta, and F.B. Malik (unpublished).
[35] I.S. Towner and J.C. Hardy, Adv. Phys. **18**, 401 (1969).
[36] N.K. Glendenning, Phys. Rev. **137**, B102 (1965).
[37] M.K. Pal, *Theory of Nuclear Structure* (Affiliated East-West Press, New Delhi, 1982).
[38] P.D. Kunz, The codes DWUCK4, DWUCK5, and CHUCK3 (private communication).
[39] N.K. Glendenning, in *Nuclear Spectroscopy and Reactions, Part D*, edited by J. Cerny (Academic, New York, 1975), p. 319.
[40] W. Fitz, J. Heger, R. Santo, and S. Wenneis, Nucl. Phys. **A143**, 113 (1970).
[41] L.A. Charlton, Phys. Rev. C **8**, 146 (1978).
[42] B.H. Wildenthal, J.B. McGrory, E.C. Halbert, and H.D. Graber, Phys. Rev. C **4**, 1708 (1971).
[43] B.H. Wildenthal and J.B. McGrory, Phys. Rev. C **7**, 714 (1973).
[44] P.M. Endt and C. van der Leun, Nucl. Phys. **A310**, 1 (1978).
[45] Gy. Bencze and J. Zimanyi, Nucl. Phys. **88**, 76 (1966).
[46] P.E. Hodgson, Oxford Report No. OUNP-94-09 (1994).